Environmental Pollution 238 (2018) 918–930

Contents lists available at ScienceDirect

Environmental Pollution

journal homepage: www.elsevier.com/locate/envpol

Impacts of transportation sector emissions on future U.S. air quality in a changing climate. Part II: Air quality projections and the interplay between emissions and climate change☆

Patrick Campbell [a, 1], Yang Zhang [a, *], Fang Yan [b, c, 2], Zifeng Lu [b, c], David Streets [b, c]

[a] *Department of Marine, Earth, and Atmospheric Sciences, NCSU, Raleigh, NC 27695, USA*
[b] *Computation Institute, University of Chicago, Chicago, IL 60637, USA*
[c] *Energy Systems Division, Argonne National Laboratory, Argonne, IL 60439, USA*

ARTICLE INFO

Article history:
Received 6 December 2017
Received in revised form
15 February 2018
Accepted 6 March 2018
Available online 24 April 2018

Keywords:
WRF/CMAQ
Transportation sector emissions
Technology Driver Model
SPEW-Trend
Climate change
Dynamical downscaling

ABSTRACT

In Part II of this work we present the results of the downscaled offline Weather Research and Forecasting/Community Multiscale Air Quality (WRF/CMAQ) model, included in the “Technology Driver Model” (TDM) approach to future U.S. air quality projections (2046–2050) compared to a current-year period (2001–2005), and the interplay between future emission and climate changes. By 2046–2050, there are widespread decreases in future concentrations of carbon monoxide (CO), nitrogen oxides ($NO_x = NO + NO_2$), volatile organic compounds (VOCs), ammonia (NH_3), sulfur dioxide (SO_2), and particulate matter with an aerodynamic diameter ≤ 2.5 μm ($PM_{2.5}$) due mainly to decreasing on-road vehicle (ORV) emissions near urban centers as well as decreases in other transportation modes that include non-road engines (NRE). However, there are widespread increases in daily maximum 8-hr ozone (O_3) across the U.S., which are due to enhanced greenhouse gases (GHG) including methane (CH_4) and carbon dioxide (CO_2) under the Intergovernmental Panel on Climate Change (IPCC) A1B scenario, and isolated areas of larger reduction in transportation emissions of NO_x compared to that of VOCs over regions with VOC-limited O_3 chemistry. Other notable future changes are reduced haze and improved visibility, increased primary organic to elemental carbon ratio, decreases in $PM_{2.5}$ and its species, decreases and increases in dry deposition of SO_2 and O_3, respectively, and decreases in total nitrogen (TN) deposition. There is a tendency for transportation emission and CH_4 changes to dominate the increases in O_3, while climate change may either enhance or mitigate these increases in the west or east U.S., respectively. Climate change also decreases $PM_{2.5}$ in the future. Other variable changes exhibit stronger susceptibility to either emission (e.g., CO, NO_x, and TN deposition) or climate changes (e.g., VOC, NH_3, SO_2, and total sulfate deposition), which also have a strong dependence on season and specific U.S. regions.

© 2018 Elsevier Ltd. All rights reserved.

1. Introduction

Rapidly changing transportation sector emissions influence atmospheric chemistry and climate, and the impacts of the emissions on air quality vary for different countries and their dominating transportation modes (Eyring et al., 2010; Lee et al., 2010; Uherek et al., 2010). Many studies have investigated the past and projected changes in the transportation sector and their emissions in developed and developing countries (e.g., Arora et al., 2011; EEA, 2012; IEA, 2014; Yan et al., 2014). Recently many retrospective studies have probed into the impacts of the transportation sector on air quality and health across the world. Bickford (2012) showed that diesel freight transport via trucks and trains contribute about 20% and 3% of all U.S. emissions of nitrogen oxides ($NO_x = NO + NO_2$) and particulate matter (PM) with an aerodynamic diameter ≤ 2.5 μm ($PM_{2.5}$), respectively, and that incorporation of biodiesel and truck-to-rail modal shifts can help reduce

---

☆ This paper has been recommended for acceptance by David Carpenter.

* Corresponding author. Department of MEAS, Campus Box 8208, Raleigh, NC 27695-8208, USA.

E-mail address: yzhang9@ncsu.edu (Y. Zhang).

[1] Currently at Computational Exposure Division, National Exposure Research Laboratory, U.S. Environmental Protection Agency, Research Triangle Park, NC, 27709, USA.

[2] Currently at Mobile Source Control Division, California Air Resources Board, Sacramento, CA 95814.

https://doi.org/10.1016/j.envpol.2018.03.016
0269-7491/© 2018 Elsevier Ltd. All rights reserved.

emissions and improve air quality in some regions. Viana et al. (2014) showed that shipping emissions in coastal regions of Europe contribute significantly to PM and nitrogen dioxide (NO_2) levels, as well as enhance new particle formation in urban areas. Other studies show that the mobile source sector is a major anthropogenic source (~21–24%) of high ozone (O_3) pollution in the summer in the Yangtze River Delta region of China (Li et al., 2015), and there are elevated $PM_{2.5}$ concentrations in near-roadway regions of southern California that contributes to a large burden of coronary heart disease mortality (Ghosh et al., 2016).

There is considerable interest in studying transportation emission changes in the future that are influenced by policy, socioeconomic, and technological drivers, and the consequences of the resulting emission changes on future regional air quality. In a review paper by Colvile et al. (2001), they summarized the impacts of air pollution from three different transportation modes (road, aircraft, and ships), discussed the immense global potential for growth of the transport sector in the future, and demonstrated the continued importance of road transportation research that has and will continue to be subjected to demand management to meet environmental objectives. Since this review, significant research has been dedicated to modeling transportation emission projections to investigate the impacts on air quality and health, and the implications for future air pollution control and policy. Through integrated transportation-land use projection modeling, McDonald-Buller et al. (2010) showed that the emissions of O_3 precursors over the large city of Austin, TX decrease dramatically by 2030 due to implementation of more stringent federal motor vehicle control programs, while the O_3 concentrations and impacts on population exposure varied in response to different policy scenarios. Implementation of Euro 3 vehicle emission standards over China may reduce emissions by more than 50% (compared to no-policy changes) of O_3 precursor gases and black (BC) and organic carbon (OC) particles, while mitigating surface O_3 and $PM_{2.5}$ concentrations by more than 10 ppb and $10\ \mu g\ m^{-3}$ in 2020 respectively (Saikawa et al., 2011). Transitioning from Tier 1 to Tier 2 emission standards for on-road gasoline-fueled light duty vehicles (both cars and trucks) in the eastern U.S. shows large benefits in reducing the absolute (relative) daily maximum 8-hr O_3 and maximum daily $PM_{2.5}$ concentrations by 16 ppb (14%) and $4.5\ \mu g\ m^{-3}$ (9%) in 2022 respectively (Vijayaraghavan et al., 2012).

To better probe the interactions between future human activities, climate change, air quality, human health, and ecosystems, the Intergovernmental Panel on Climate Change (IPCC) research community has developed two popular sets of scenarios that are based on expert judgments of plausible future emissions considering socioeconomic, environmental, and technological trends. These include 1) the Special Report on Emissions Scenarios (SRES; Nakicenovic et al., 2000), and 2) the Representative Concentration Pathways (RCP; Moss et al., 2010). Both the IPCC SRES and RCP scenarios have their own uncertainties in the projections, and there are both similarities and differences between the scenario families (Rogelj et al., 2012). Using RCP4.5 and 8.5 scenarios, Baklanov et al. (2010) assessed the effects of future climate change on air quality, as well as climate change impacts on the policy measures designed for reducing the health impacts of transportation sector emissions. They showed that the direct impacts of climate change on air quality near major cities in Europe include enhancements in strong winds in mid-latitude high and low pressure systems, in conjunction with suppressed mixing will lead to strong long-range, near-surface export of pollutants. Baklanov et al. (2010) also indicated that the RCP8.5-predicted increases in temperature and photolysis are expected to increase near-surface O_3 levels in the future, but that the increases will be outweighed by the expected decline in the emissions of O_3 precursor gases due to transportation in Europe. Penrod et al. (2014) used dynamically downscaled climate model output and regional all-sector emission changes over the U.S. based on the SRES A1B family scenario, and showed that increased temperatures lead to increases of up to 5 ppb in maximum 8-hr average O_3 in the winter over the U.S., and the large reductions in NO_x emissions drive decreases in O_3 over most of the U.S. during summer. Also, Penrod et al. (2014) showed that significant emission reductions dominate the climate change impacts on future $PM_{2.5}$ concentrations over the U.S.

The emission projections in previous work did not account for explicit relationships between socioeconomic factors and technology changes (Yan et al., 2014), and also simply assumed that the emission projections are the same across the entire domain used in the air quality modeling system. It is essential to more accurately differentiate emitters by their emission characteristics that are continually influenced by dynamic changes in technology (i.e., economic development, policy changes, and emission control strategies), while determining the emission factors using explicit relationships rather than by expert judgments (Yan et al., 2014). It is also beneficial to combine the emission changes in short-lived species from the transportation sector, with simultaneous increases in the long-lived greenhouse gases (GHGs) such as methane (CH_4) and carbon dioxide (CO_2), as these gases also have direct and indirect effects on air pollutant concentrations, and thus more appropriately represent possible future scenarios. The spatial, temporal, and socioeconomic-technological relationship variabilities in future emission projections can have important impacts on the predicted air quality changes in the future, especially when combined with variability in regional climate change impacts.

Over the past 30 years there are increasing trends in total U.S. population, vehicles miles traveled, energy and fuel consumption, and gross domestic product; however, air pollutant emissions and concentrations have shown decreasing trends due to implementation of dynamic technological changes in the transportation sector (Yan et al., 2014). In the future, the impacts of changing transportation emissions involve a complex interplay between socioeconomic-technological-driven changes and the global and regional influences of climate change in the U.S., both of which may include spatial and seasonal variability across different regions. In Part I of this work (Campbell et al., 2018), we provided an overview of the advanced Technology Driver Model (TDM) approach (see graphical abstract in Part I), explained the dynamically downscaled air quality modeling system configuration and design summary, detailed and quantified the dynamic transportation sector emission changes from the Speciated Pollutant Emission Wizard-Trend (SPEW-Trend) model over the U.S., and comprehensively evaluated the model system. In this Part II, we use the transportation emission projections from Part I and quantify their impacts on future U.S. air quality in the face of future climate and GHG changes (Section 2), and then summarize the important results (Section 3).

2. Projected air quality changes over the U.S. by 2046–2050

This section presents the projected U.S. air quality changes due to transportation sector emissions (Part I) and the interplay among emission, GHG, and climate changes. To do this, a 5-year current (2001–2005) and future (2046–2050) period from a Community Climate System Model (CCSM) simulation is dynamically downscaled and provides the initial (ICONs) and boundary conditions (BCONs) for the IPCC A1B scenario to the Weather Research and Forecast version 3.6.1, which then drives the offline Community Multiscale Air Quality model version 5.0.2 (WRF_CCSM/CMAQ) model (see Part I, Section 2 for more details). Table 1 summarizes the six WRF_CCSM/CMAQ sensitivity simulation sets.

These consist of 1) a current-year 2001–2005 period (CURR),

Table 1
Summary of the six WRF/CMAQ sensitivity simulation sets conducted in this study, their abbreviations/acronyms used in the text, and additional details regarding their impacts on future U.S. air quality.

WRF/CMAQ Simulation Sets		Descriptions	
Run#	Run Details *Current = 2001–2005* *Future = 2046–2050 A1B*	Abbreviation	Impacts on Future U.S. Air Quality
1	Current Climate Current Greenhouse Gas (GHG) Levels Current Emissions	CURR	None
2	Current Climate Future GHG Levels Future On-Road Vehicle (ORV) Emissions	ORV_GHG	Combined future GHG and ORV changes
3	Current Climate Future GHG Levels Future Non-Road Engine (NRE) Emissions	NRE_GHG	Combined future GHG and NRE changes
4	Current Climate Future GHG Levels Future Total Transportation (TT) Emissions	TT_GHG	Combined future GHG and TT changes
5	Future Climate Future GHG Levels Future TT Emissions	TT_CC	Combined future climate, GHG, and TT changes
6	Current Climate Current GHG Levels Future TT Emissions	TT_Only	Future TT changes only

and future-year 2046–2050 A1B runs that incorporate 2) on-road vehicle (ORV) emission and GHG changes (ORV_GHG), 3) non-road engine (NRE) emission and GHG changes (NRE_GHG), 4) total transportation (TT) emission and GHG changes (TT_GHG), 5) TT emission, GHG, and climate changes (TT_CC), and 6) TT emission changes only (TT_Only). We note that ORV consists of light-duty diesel, heavy-duty diesel, and light-duty gasoline vehicles, NRE consists non-road diesel and gasoline vehicles, and shipping, rail, and aircraft are treated as separate transportation emission modes. Thus ORV + NRE do not equal TT emissions. We further note that the WRF runs (1)–(4) and (6) use current climate CO_2 and CH_4 mixing ratios of 340 and 1.85 ppm, while run (5) uses future climate values of 785 and 3.33 ppm respectively. The CMAQ runs (1) and (6) use the aforementioned current CO_2 and CH_4 mixing ratios, while runs (2)–(5) use the future mixing ratio values. Thus comparing the WRF/CMAQ output from (1) to the output from (2) through (4) shows the direct impacts of GHG and transportation emission projections (Section 2.1). Comparing (4) and (5) investigates the interplay between emission changes, climate changes, and their relative impacts on future air quality (Section 2.2), while also estimating (i.e., neglecting non-linear effects) the impacts of climate change only (CC_only* ~ (5)–(4)). Finally, comparing (4) and (6) demonstrates the relative impacts of TDM transportation emission changes versus longer-lived, energy-related, GHG changes (e.g., CO_2 and CH_4) on future U.S. air quality (Section 2.2).

2.1. *Impacts of transportation emission projections*

In this subsection, we present the results of CURR and ORV_GHG, NRE_GHG, and TT_GHG sensitivity simulations (Table 1) that are designed to reveal the impact (and separate the effects) of ORV, NRE, and TT emission and GHG changes on future U.S. air quality. From these simulations, we show the specific impacts of such transportation emission and GHG changes on gas and aerosol concentrations (Subsection 2.1.1), primary organic and elemental carbon (Subsection 2.1.2), haze and visibility (Subsection 2.1.3), and dry and wet deposition (Subsection 2.1.4).

2.1.1. *Gas and aerosol concentrations*

Fig. 1 shows spatial plots of the annual average current year (2001–2005) mixing ratios (ppb) of carbon monoxide (CO), NO_x, total volatile organic compounds (VOCs), maximum daily average 8-hr (MDA8) O_3, ammonia (NH_3), and sulfur dioxide (SO_2), and their absolute changes (Δ ppb) in the future (2046–2050) for the ORV_GHG, NRE_GHG, and TT_GHG simulations.

There are significant decreases in future CO, NO_x, and VOCs annual mixing ratios near urban centers for ORV_GHG (Fig. 1g–i), which are especially widespread for NO_x, but there are also some increases in VOCs over the southern half of CONUS, especially over Florida (Part I). The widespread decreases are impacted by a combination of more stringent regulations and decreases in fuel consumption, which lead to widespread future decreases in ORV emissions for these gases relative to 2001–2005, especially near the urban centers (Part I). Decreases in CO, NO_x, and VOCs mixing ratios have also been shown in recent studies that use future global RCP8.5 emission projections incorporated into downscaled WRF with Chemistry (WRF/Chem) simulations over a similar CONUS domain for 2046–2055 (Yahya et al., 2017); however, due to less spatial detail in the regional RCP emission projections compared to TDM, the RCP study showed less spatial variability in the future decreases in CO, NO_x, and VOC over the U.S., and less defined maxima in the vicinity of the urban centers. We note that the global RCP8.5 emission projections consider additional sector changes (e.g., residential, agriculture, industry, and power); while here the focus is on the transportation sector emission changes only. Increases in future background CH_4 for the A1B scenario lead to regional increases in MDA8 O_3 for ORV_GHG (Fig. 1j), especially in the eastern U.S. and in California, with even more significant increases (max ~ + 11 ppb) near the urban centers due to larger reductions in ORV NO_x emissions compared to those in VOC emissions (Part I) near the VOC-limited regions. There are also decreases in NH_3 and SO_2 due to decreasing ORV emissions near cities with a high population density (Fig. 1k–l).

The NRE_GHG decreases are significantly less for all gas mixing ratios (Fig. 1m–q), except for SO_2 (Fig. 1r), which has slightly greater decreases. In fact, there are predominant increases in VOCs for NRE_GHG, largely due to increases in VOC emissions from non-road gasoline engines (Part I). This leads to more widespread MDA8 O_3 increases in the eastern U.S. (Fig. 1p) due to widespread increases in VOCs and decreases in NO_x over VOC-limited regions. The

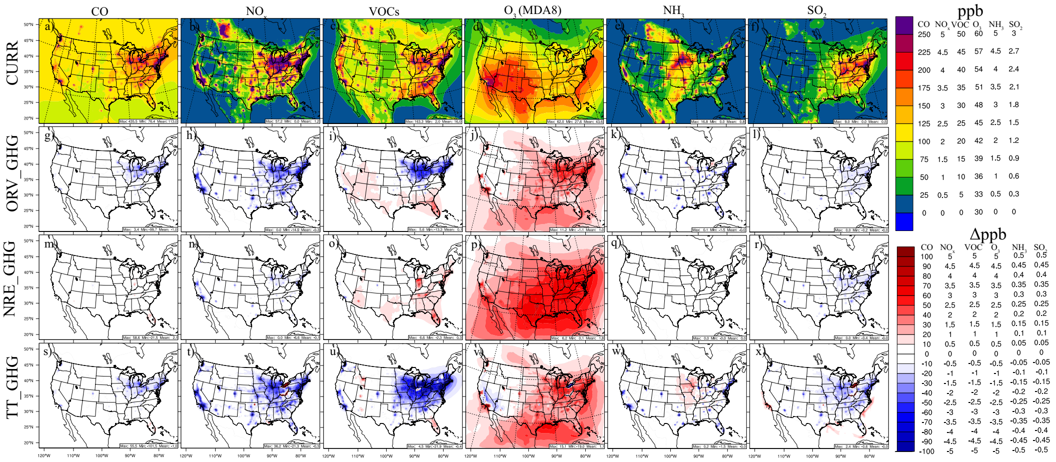

Fig. 1. Spatial plots of annual (January–December) average current year period (2001–2005) gaseous mixing ratios of CO, NO_x, total VOCs, O_3 (Maximum Daily Average 8-hr; MDA8), NH_3, and SO_2 (row 1; a–f), and their future year period (2046–2050) absolute (future − current) changes for the ORV_GHG (row 2; g–l), NRE_GHG (row 3; m–r), and TT_GHG (row 4; s–x) simulations under the A1B scenario. Spatial plots of annual average relative percent changes are shown in Supplementary Fig. S1, and seasonal average relative percent changes are shown in Supplementary Figs. S2–S5.

NRE_GHG has less NO_x reduction (Fig. 1n) compared to ORV_GHG (Fig. 1h) in the high NO_x regions of the eastern U.S., which leads to comparably larger and widespread increases of O_3 via the CH_4 oxidation pathway in the NRE_GHG simulation (see Section 2.2.4). The ORV_GHG (Fig. 1s–x) impacts dominate the TT_GHG decreases in CO, NO_x, VOCs in the northeast U.S., and NH_3, while both the ORV_GHG and NRE_GHG contribute to the decrease in SO_2 for TT_GHG rather equally. There are, however, additional impacts from changes in other transportation modes in TT_GHG, including increases in NO_x and SO_2 due to projected increases in shipping emissions, which becomes more apparent in the relative percent changes in TT_GHG shown in Supplementary Fig. S1. There are also large relative decreases in NO_x and SO_2 in the western U.S. for TT_GHG that are not evident in either the ORV_GHG or NRE_GHG modes (Fig. S1). These changes are dominated by decreases in locomotive emissions near major railways (Yan et al., 2014).

The widespread increases in MDA8 O_3 for TT_GHG in the eastern U.S. and in California are strongly impacted both by the ORV_GHG and NRE_GHG changes, with large increases near the local urban centers; however, the spatial pattern of ORV_GHG matches most closely to the TT_GHG in the eastern U.S., with even less increases (or decreases) in MDA8 O_3 in the western U.S. This indicates that the larger decreases in NO_x for ORV_GHG compared to NRE_GHG in the eastern U.S., and even further decreases in NO_x in the western U.S. for TT_GHG due to other transportation modes (e.g., locomotives), strongly impact the regional NO_x-limited O_3 chemistry and spatial patterns of MDA8 O_3 decreases across CONUS. There are some local decreases in MDA8 O_3 due to local increases in NO_x near major waterways (from increased shipping emissions of NO_x), which are mainly characterized by VOC-limited O_3 chemistry. There are other regions over California and Nevada that display decreases in MDA8 O_3 for TT_GHG, which are due to overall larger decreases in NO_x compared to the decreases (or increases) in VOCs in NO_x-limited areas that are predicted by many air quality models (e.g., Fig. 4 in Campbell et al., 2015).

In Part I, there are clear indications of seasonal changes in the TDM emission projections for many gas species, especially for the NREs (Part I; Figs. S2–S5). This factor in conjunction with seasonal changes in climatic conditions for different regions of CONUS, lead to a seasonal variability in relative percent changes for many of the gas species. Decreases in CO, VOC, NO_x, NH_3 and SO_2 are the largest and most widespread across CONUS in the winter season for ORV_GHG, NRE_GHG, and TT_GHG. The relatively large percent increases in NH_3 in winter for ORV_GHG and TT_GHG are due to small NH_3 increases relative to small current year NH_3 amounts in this season and U.S. regions. The largest increases in O_3 are found near the VOC-limited regions in winter and fall due to larger decreases of NO_x compared to smaller decreases (or increases) in VOC, especially for ORV_GHG and TT_GHG.

Fig. 2 shows spatial plots of the annual average current year (2001–2005) mass concentrations (μg m^{-3}) of $PM_{2.5}$, sulfate (SO_4^{2-}), nitrate (NO_3^-), ammonium (NH_4^+), organic matter (OM = 1.4*organic carbon (OC)), elemental carbon (EC), and secondary organic aerosol (SOA), and their absolute changes (Δ μg m^{-3}) in the future (2046–2050) for the ORV_GHG, NRE_GHG, and TT_GHG simulations.

There are widespread decreases in $PM_{2.5}$ and most species across CONUS, especially in the eastern U.S. An exception are small increases in OM an-d SOA in the eastern U.S. The TT_GHG changes in $PM_{2.5}$ and species are dominated by the ORV_GHG changes, except for OM and EC, which has significant contributions of both ORV_GHG and NRE_GHG changes to the TT_GHG changes. The decreases in $PM_{2.5}$ and species are due to widespread decreases in primary PM emissions from both ORVs and NREs, especially for primary EC (PEC) emissions, as well as decreases in precursor gas emissions that are dominated by ORVs for NO_x and NH_3 (Part I; Campbell et al., 2018). The largest contribution to the TT_GHG decreases in total $PM_{2.5}$ are from to NO_3^- and EC decreases. There are also local increases in OM and EC found near major waterways due to an increase of PM emissions from shipping. The increases in SOA are due to increases in VOCs mixing ratios from increases in VOCs emissions mainly from NREs (Part I).

The decreases in $PM_{2.5}$ and species are relatively small compared to the gas species for TT_GHG, where the average decrease in $PM_{2.5}$ over CONUS is about -0.2 μg m^{-3}, and the largest decrease is -2.4 μg m^{-3} (Fig. 2v). The annual relative percent differences in total $PM_{2.5}$ and most species are also small on average (within ±5%) compared to the current-year levels, except for NO_3^- and EC that both have average decreases of about −22%. There is less seasonal variability for $PM_{2.5}$ and species (Figs. S7–S10) compared to many of the gas species; however, there are relatively larger decreases in NO_3^- and EC that occur in the summer and fall seasons due to ORV and NRE emission changes, respectively.

The remaining parts of Section 2.1 pertain to analyses of

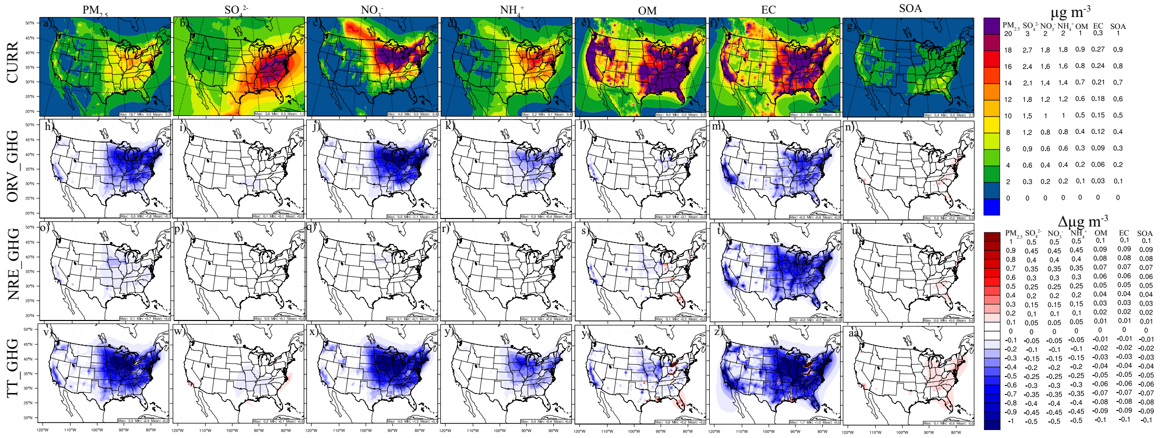
PM2.5
SO4 2-
NO3 -
NH4 +
OM
EC
SOA
CURR
ORV_GHG
NRE_GHG
TT_GHG
a)
b)
c)
d)
e)
f)
g)
h)
i)
j)
k)
l)
m)
n)
o)
p)
q)
r)
s)
t)
u)
v)
w)
x)
y)
z)
aa)
μg m-3
PM2.5 SO4 2- NO3 - NH4 + OM EC SOA
20 3 2 2 1 0.3 1
18 2.7 1.8 1.8 0.9 0.27 0.9
16 2.4 1.6 1.6 0.8 0.24 0.8
14 2.1 1.4 1.4 0.7 0.21 0.7
12 1.8 1.2 1.2 0.6 0.18 0.6
10 1.5 1 1 0.5 0.15 0.5
8 1.2 0.8 0.8 0.4 0.12 0.4
6 0.9 0.6 0.6 0.3 0.09 0.3
4 0.6 0.4 0.4 0.2 0.06 0.2
2 0.3 0.2 0.2 0.1 0.03 0.1
0 0 0 0 0 0 0
Δμg m-3
PM2.5 SO4 2- NO3 - NH4 + OM EC SOA
1 0.5 0.5 0.5 0.1 0.1 0.1
0.9 0.45 0.45 0.45 0.09 0.09 0.09
0.8 0.4 0.4 0.4 0.08 0.08 0.08
0.7 0.35 0.35 0.35 0.07 0.07 0.07
0.6 0.3 0.3 0.3 0.06 0.06 0.06
0.5 0.25 0.25 0.25 0.05 0.05 0.05
0.4 0.2 0.2 0.2 0.04 0.04 0.04
0.3 0.15 0.15 0.15 0.03 0.03 0.03
0.2 0.1 0.1 0.1 0.02 0.02 0.02
0.1 0.05 0.05 0.05 0.01 0.01 0.01
0 0 0 0 0 0 0
-0.1 -0.05 -0.05 -0.05 -0.01 -0.01 -0.01
-0.2 -0.1 -0.1 -0.1 -0.02 -0.02 -0.02
-0.3 -0.15 -0.15 -0.15 -0.03 -0.03 -0.03
-0.4 -0.2 -0.2 -0.2 -0.04 -0.04 -0.04
-0.5 -0.25 -0.25 -0.25 -0.05 -0.05 -0.05
-0.6 -0.3 -0.3 -0.3 -0.06 -0.06 -0.06
-0.7 -0.35 -0.35 -0.35 -0.07 -0.07 -0.07
-0.8 -0.4 -0.4 -0.4 -0.08 -0.08 -0.08
-0.9 -0.45 -0.45 -0.45 -0.09 -0.09 -0.09
-1 -0.5 -0.5 -0.5 -0.1 -0.1 -0.1
120°W
110°W
100°W
90°W
80°W

Fig. 2. Spatial plots of annual (January–December) average current year period (2001–2005) mass concentrations of $PM_{2.5}$, SO_4^{2-}, NO_3^-, NH_4^+, OM, EC, and SOA (row 1; a–g), and their future year period (2046–2050) absolute (future − baseline) changes for the ORV_GHG (row 2; h–n), NRE_GHG (row 3; o–u), and TT_GHG (row 4; v–aa) simulations under the A1B scenario. Spatial plots of annual average relative percent changes are shown in Supplementary Fig. S6, and seasonal average relative percent changes are shown in Supplementary Figs. S7–S10. Nearly identical results for $PM_{2.5}$ and species changes for TT_Only (No GHG) case are shown in Supplementary Fig. S40.

ORV_GHG, NRE_GHG, and TT_GHG changes in primary OC to EC ratio (Section 2.1.2), haze and visibility (Section 2.1.3), and dry and wet deposition (Section 2.1.4), which largely follow changes in their associated air quality variables in Figs. 1 and 2. Thus although these changes are important and are further detailed below, their associated figures are found in Supplementary Sections 1–5.

2.1.2. *Primary organic and elemental carbon*

The changes in the OC and EC due to primary PM emission changes lead to changes in the future primary OC to EC ratio, $(OC/EC)_{pri}$, which is a useful parameter in identifying primary fossil fuel combustion sources, as EC can be used as a tracer to track the portion of co-emitted primary OC (i.e., the EC tracer method; Turpin and Huntzicker, 1995; Cabada et al., 2004). Considering that EC is exclusively associated with primary emissions, the EC tracer method can also differentiate OC from primary and secondary sources when $(OC/EC)_{pri}$ is compared to ambient OC/EC ratios (e.g., Turpin et al., 1991; Wu and Yu, 2016). Thus the projected changes in $(OC/EC)_{pri}$ for different regions are important in probing OC aging processes and for developing future effective emission control policies. Fig. S41 shows the annual average current and projected changes in the $(OC/EC)_{pri}$ ratio for ORV_GHG, NRE_GHG, and TT_GHG.

The decreases in primary ORV, NRE, and other transport mode (i.e., ship, rail, and aircraft) emissions of EC lead to widespread decreases in EC concentrations for ORV_GHG, NRE_GHG, and TT_GHG, especially in the eastern U.S. The decreases in EC, as well as some increases in OM in the eastern U.S., lead to predominantly increasing $(OC/EC)_{pri}$ across the U.S. in the future, with domain-wide average values of 1.8, 2.0, 2.0, and 2.3 for CURR, NRE_GHG, ORV_GHG, and TT_GHG, respectively. There is a clear seasonal dependence on the $(OC/EC)_{pri}$ for CURR (Figs. S11a–S11d), and the domain-wide averages are 2.1, 1.6, 1.5, and 1.8 for the winter, spring, summer, and fall respectively. There is also some moderate seasonal dependence on the projected change in $(OC/EC)_{pri}$, where for ORV_GHG (Figs. S11e–S11h), NRE_GHG (Figs. S11i–S11l), and TT_GHG (Figs. S11m–S11p) the absolute (relative) increases in the domain-wide average $(OC/EC)_{pri}$ have a seasonal range of about 0.1–0.2 (7–11%), 0.1–0.3 (6–17%), and 0.3–0.6 (19–33%) respectively. The seasonality in the projected $(OC/EC)_{pri}$ changes are predominantly driven by the seasonal EC concentration changes discussed above.

2.1.3. *Haze and visibility*

The projected change in future $PM_{2.5}$ and its species concentrations also has impacts on haze and visibility across CONUS, as shown in the current and projected changes in the deciview (dv) haze index for CURR, NRE_GHG, ORV_GHG, and TT_GHG in Fig. S42.

The use of dv as a haze index was introduced by Pitchford and Malm (1994), where the dv was derived to present data relating the light-extinction coefficient of ambient air to human perceptibility of haze or visibility impairment. The dv haze index is near zero for a pristine atmosphere, and increases as visibility is degraded. Decreases in $PM_{2.5}$ concentrations due to decreases in ORV, NRE, and other transportation mode primary PM and precursor gases result in a decrease in domain-wide average (minimum) dv of about −0.2 (−1.6), −0.1 (−0.4), and −0.2 (−1.9) for ORV_GHG (Fig. S42b), NRE_GHG (Fig. S42c), and TT_GHG (Fig. S42d), respectively. There is moderate seasonality in the relative % change in dv, with slightly larger domain-wide average dv decreases in the winter (~−3%) compared to other seasons for ORV_GHG and TT_GHG. Pitchford and Malm (1994) and the U.S. Environmental Protection Agency (EPA) (EPA, 2007) noted that a change of 1 dv (~10% extinction coefficient) may be perceived as a small but noticeable change in haziness under most circumstances. Thus the annual dv decreases by as much as −1.9 for TT_GHG in Fig. S42d indicate that the projected PM emission decreases in the transportation sector (mainly from the ORV mode), while although relatively small compared to the gas species, may have a perceived improvement in future visibility that is most prolific in the eastern half of the U.S.

2.1.4. *Dry and wet deposition*

Fig. S43 shows spatial plots of the annual average current year (2001–2005) dry deposition (g ha^{-1}) of SO_2 ($DDEP\_SO_2$), O_3 ($DDEP\_O_3$), NH_3 ($DDEP\_NH_3$), nitric acid ($DDEP\_HNO_3$), and total nitrogen (DDEP_TN[3]), and their absolute changes (Δ g ha^{-1}) in the future (2046–2050) for the ORV_GHG, NRE_GHG, and TT_GHG simulations. Dry deposition is generally calculated in air quality models as the product of the species concentration in the atmosphere (assuming a zero concentration at the surface) and a deposition velocity, V_d. In CMAQ, V_d is computed using an electrical resistance (R) analog model (Pleim et al., 2001; Pleim and Ran, 2011) that uses calculated aerodynamic (R_a), boundary-layer diffusion (R_b), and surface resistances (R_s). The calculation of V_d values in CMAQ makes use of surface and surface-layer parameters (e.g., leaf-area index, fractional vegetation cover, canopy water content, bulk stomatal resistance (R_{st}), R_a, and roughness length) generated by the land surface model (LSM), if available, that is within WRF. In the case of the Noah LSM used here (see Table 2 in Part 1), some of the near-surface and surface fields necessary for the V_d calculation in CMAQ are unavailable in the WRF meteorological output. Therefore, they must be internally calculated using the Meteorology-Chemistry Interface Processor (MCIP) for offline CMAQ with algorithms that are independent of the Noah LSM, which results in additional inconsistencies. The change in projected dry deposition may be impacted by source emission changes that can change species' ambient concentrations (and chemistry), and/or surface and near-surface parameter changes that impact R_a and R_s and the resulting V_d calculation in CMAQ for each species. In Fig. S43, however, only emission and GHG changes are considered, and only the changes in emissions and resulting atmospheric concentrations may impact the projected dry deposition rates. Thus the projected DDEP_SO_2, DDEP_O_3, DDEP_NH_3, DDEP_HNO_3, DDEP_TN changes for ORV_GHG (Figs. S43f–S43j), NRE_GHG (Figs. S43k–43o), and TT_GHG (Figs. S43p–S43t) are primarily driven by the changes in their respective concentrations, and the spatial distribution of absolute (relative) changes in the dry deposition fluxes in Fig. S43 (Fig. S13) qualitatively agrees with the changes in the mixing ratios of associated species in Fig. 1 (Fig. S2). Furthermore, the seasonal relative changes in dry deposition (Figs. S14–S17) also compare closely to the associated gas concentration changes (Figs. S2–S5). The overall increases in DDEP_O_3 may be detrimental due to increases in the O_3 dose to leaf interiors where the damage occurs, whereas the future decreases in DDEP_SO_2 and DDEP_TN deposition over CONUS may have a positive benefit in reducing the impacts of acidification and nutrient enrichment (i.e., eutrophication) on terrestrial and aquatic ecosystems. There are increases in DDEP_SO_2 over some major waterways due to increased shipping emissions of SO_2, and this may lead to an increase in acidification in these regions.

---

[3] $TN = NO_3^-(i,j,k) + 0.984*HNO_3 + NO_3 + 3.647*NH_3 + 3.444*NH_4^+(i,j,k) + 0.512*PAN + 1.148*N_2O_5 + 1.319*HONO$; where i, j, and k refer to the Aitken, accumulation, and coarse aerosol modes.

The DDEP_NH_3 rates are also impacted by the bi-directional (BIDI) exchange of NH_3 (i.e., NH_3 deposition or emission; BIDI-NH_3) that is implemented in CMAQ (see Table S1 in Part I; Cooter et al., 2012; Bash et al., 2013), although the transportation emission changes in NH_3 are relatively small compared to other gas constituents. In the case of BIDI-NH_3, the surface concentration of NH_3 is not necessarily zero, and may be different for various types of the surface such as the ground and vegetation canopy. Depending on the NH_3 compensation point concentrations in the surface canopy and the air above, the NH_3 may flux to or from the surface. BIDI-NH_3 processes can exhibit significant spatial (e.g., near heavy fertilizer applications and livestock operations), and temporal (e.g., diurnal to seasonal) variability, and thus may modulate the future DDEP_NH_3 changes.

Fig. S44 shows spatial plots of the annual average current year (2001–2005) wet deposition (g ha^{-1}) of total sulfate (WDEP_TSO_4^{2-}),[4] TN (WDEP_TN), and total ammonium (WDEP_NH_x),[5] and their absolute changes (Δ g ha^{-1}) in the future (2046–2050) for the ORV_GHG, NRE_GHG, and TT_GHG simulations.

For similar reasons described in the dry deposition changes in Fig. S43, the wet deposition changes are largely driven by the total PM concentration changes (inferring in-cloud concentrations), as wet deposition rates are an integral of the product of the in-cloud concentration and the precipitation rate, in which the latter does not change in ORV_GHG, NRE_GHG, or TT_GHG in Fig. S44. The small increases in SO_2 and SO_4^{2-} concentrations in parts of the eastern U.S. and just offshore (due to shipping emission increases) lead to enhanced SO_4^{2-} cloud chemistry and resulting small increases in WDEP_TSO_4^{2-} for ORV_GHG, NRE_GHG, and TT_GHG. There are predominant decreases in WDEP_TN in the eastern U.S., largely dominated by ORV_GHG changes in NO_3^- concentrations due to decreases in ORV emissions of NO_x. The increases in WDEP_NH_x in central CONUS are driven by increases in NH_3 and NH_4^+ concentrations for both ORV_GHG and NRE_GHG, while the decreases in the eastern U.S. are mainly driven by decreases in ORV_GHG. It is worth noting that like the PM concentration changes, the relative changes in wet deposition are rather small (within ±5%) compared to the current year values, with the exception of the WDEP_TN and WDEP_NH_x decreases in the east and west U.S. (Fig. S18), and the seasonality of wet deposition (Figs. S19–S22) matches the spatial patterns of the relative PM concentration changes.

2.2. Interplay between emission and climate changes

In this subsection, we present the results of TT_CC, TT_Only, and CC_Only* (i.e., TT_CC − TT_GHG) sensitivity simulations (Table 1) that are designed to reveal the interplay (i.e., separate and combined effects) of total transportation emission, climate, and GHG changes on future U.S. air quality. From these simulations, we first show the downscaled future climate changes for the A1B scenario (Subsection 2.2.1), and then the specific interplay and impacts of transportation emission, climate, and GHG changes on gas and aerosol concentrations (Subsection 2.2.2), total sulfate and nitrogen deposition (Subsection 2.2.3), emissions vs. greenhouse gas impacts on ozone and PM (Subsection 2.2.4), and the implications on for future O_3 and $PM_{2.5}$ levels over the U.S (Subsection 2.2.5).

2.2.1. Future climate changes for A1B scenario

Fig. 3 shows spatial plots of the annual average current year (2001–2005) 2-m temperature (T2, °C), 10-m wind speed (WS10, m s^{-1}), planetary boundary layer height (PBLH, m), cloud fraction (CFRAC), downward shortwave radiation at the ground (GSW, W m^{-2}), and total rain (RT, mm day^{-1}), as well as their absolute changes in the future (2046–2050).

As typical with the IPCC A1B scenario and enhanced GHG levels, there is widespread warming and an increase in wind speed across the entire CONUS in the future, in this case with a domain-wide mean (maximum) increase in T2 and WS10 of about 1 °C (3.4 °C) and 0.1 m s^{-1} (1.0 m s^{-1}). Regions of western and northern U.S. and southern Canada experience some of the greatest warming by 2046–2050. The increases in T2 and WS10 also lead to widespread mean (maximum) increases in the PBLH of about 23 m (141 m). The decreases in 2-m water vapor mixing ratio (figure not shown) also lead to widespread decreases in CFRAC, especially in the eastern U.S. The widespread decreases in CFRAC in the eastern U.S. lead to increases in GSW, especially in the southeastern U.S., but there are some areas in the western U.S. that exhibit relatively small increases in CFRAC and decreases in GSW. Changes in RT are somewhat more complex, but there is an apparent dipole of decreased RT in the southeast, and increased RT in the northwest U.S. There are significant impacts of the CCSM ICONs and BCONs on the decreases in moisture and precipitation formation in the southeast

---

[4] $TSO_4^{2-} = SO_4^{2-}(i,j,k) + 1.5*SO_2$; where i, j, and k refer to the Aitken, accumulation, and coarse aerosol modes.

[5] $NH_x = NH_4^+(i,j,k) + 1.059*NH_3$; where i, j, and k refer to the Aitken, accumulation, and coarse aerosol modes.

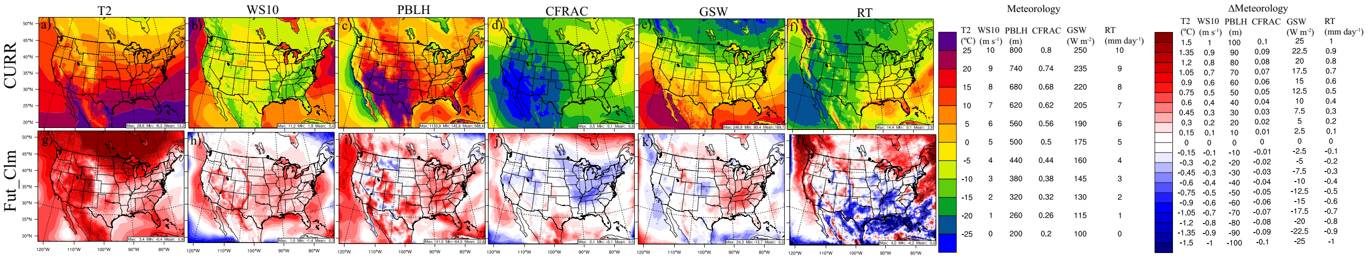

Fig. 3. Spatial plots of annual (January–December) average current year period (2001–2005) T2 (°C), WS10 (m s^{-1}), PBLH (m), CFRAC, GSW (W m^{-2}), and RT (mm day^{-1}) (row 1; a–f), and their future year period (2046–2050) absolute (future − current) changes under the A1B scenario (row 2; g–l). Spatial plots of annual average relative percent changes are shown in Supplementary Fig. S23, and seasonal average relative percent changes are shown in Supplementary Figs. S24–S27.

U.S., which largely stem from a rather low moisture flux from the southern boundary of the domain and the Gulf of Mexico (not shown). Yahya et al. (2017) showed similar annual average spatial patterns of T2, WS10 and PBLH increases by 2046–2054 that are somewhat larger (smaller) in magnitude for T2 (WS10 and PBLH) for downscaled RCP8.5 WRF simulations over CONUS.

There is strong seasonal variability (Figs. S24–S27) in the relative percent changes of some meteorological variables compared to the annual average percent change (Fig. S23). For T2, there are widespread decreases (increases) in southern (northern) U.S. during winter, and widespread increases in spring, summer, and fall across the entire U.S. The fall and winter seasons exhibit the largest increases for WS10 and PBLH across CONUS, and there are also some large areas of increased (decreased) CFRAC (GSW) in the winter, spring, and fall. In summer, there is strongly decreased CFRAC and RT but increased GSW across all of CONUS, especially in the western and eastern U.S. There are larger increases in RT in the winter, spring, and fall, peaking in the winter in the southern U.S., which is coincident with increases in water vapor mixing ratio (not shown) and CFRAC in this region and season. A strong cyclonic (anticyclonic) large-scale pressure dipole is predicted in the eastern (western) U.S. in 2046 compared to 2001 (not shown) and strongly impacts the 5-year annual average changes, which is further amplified when analyzing the seasonal changes. Winter to summer seasonal variability in near future (2026–2030) changes in CCSM downscaled WRF meteorological variables were also apparent in Penrod et al. (2014), e.g., widespread precipitation increases in the winter and decreases in the summer.

2.2.2. *Gas and aerosol concentrations*

Fig. 4 provides similar annual average absolute difference plots of gas mixing ratios as in Fig. 1, but for the TT_CC (total emissions + climate changes) and approximated CC_Only* (climate change only) simulations, as well as a relative impact ratio (brown = emissions dominant, blue = climate dominant) defined as the ratio of the changes in absolute values of CC_Only* to the absolute values of TT_GHG (total emissions only) changes (i.e., |ΔCC_Only*|/|ΔTT_GHG|).

For CO and NO_x, it is clear that where the TT_CC decreases are the greatest, they are dominated by transportation emission changes, with minimal influences from climate change, especially for NO_x. However, there is considerably more influence from climate changes on VOCs, O_3 (MDA8), and NH_3. Where the changes are at their greatest, the VOC increases are strongly impacted by increased temperatures and contribution from enhanced biogenic VOCs (BVOCs) near the heavily vegetative regions (e.g., southeast and west-northwest U.S.). While there is some contribution to VOC decreases from CC_Only*, there are many regions of decreases that are dominated by the emission changes as well. Interestingly, the impact of CC_only* results in decreased O_3 in most of the central and eastern U.S., and increased O_3 in the northwest. The relatively smaller warming (or even some cooling) regions in the central and eastern U.S., combined with the effect of consistent enhancements in PBLH (from enhanced WS10) in these regions lead to decreases in near-surface O_3 to first order. Emission changes (and enhanced CH_4) dominate the O_3 increases in much of the Midwest and eastern U.S. (brown colors in Fig. 4p) as climate effects are offsetting (weak warming but enhanced PBLH). The relatively larger warming

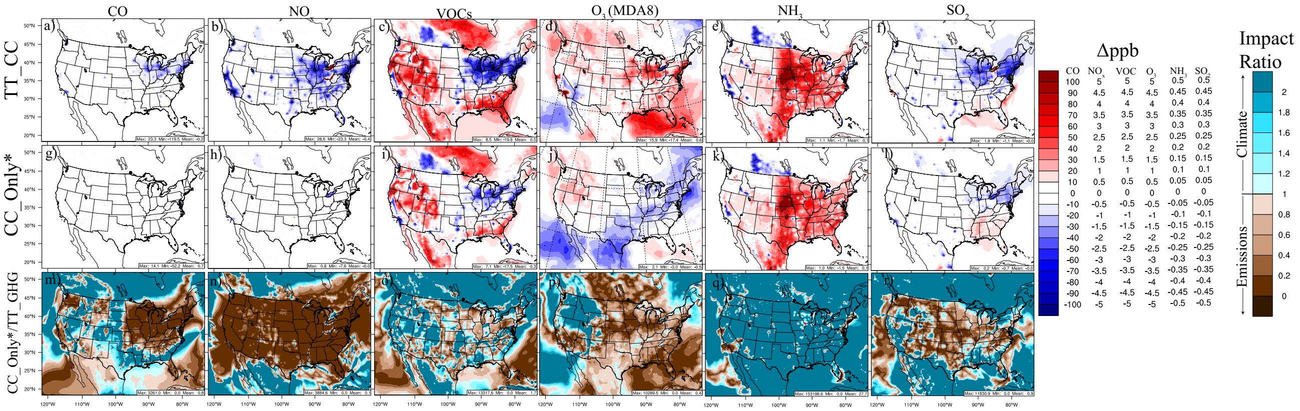

Fig. 4. Spatial absolute (future − current) difference plots of annual (January–December) average gas mixing ratios of CO, NO_x, total VOCs, O_3 (Maximum Daily Average 8-hr; MDA8), NH_3, and SO_2 for TT_CC (row 1; a–f), CC_Only* (row 2; g–l), and an approximate emission vs. climate change impact ratio defined as |ΔCC_Only*|/|ΔTT_GHG| (row 3; m–r) under the A1B scenario. Brown colors indicate dominancy of the impacts of emission changes, while blue indicates dominancy of the impacts of climate changes. Spatial plots of annual average relative percent changes are shown in Supplementary Fig. S28, and seasonal average relative percent changes are shown in Supplementary Figs. S29–S32. (For interpretation of the references to color in this figure legend, the reader is referred to the Web version of this article.)

(and enhanced BVOCs - not shown) in conjunction with many areas of decreased PBLH in the west and northwest U.S. results in climate changes dominating compared to the impacts of reductions of precursor emissions and GHGs (blue colors in Fig. 4p), and consequently O_3 increases in the northwest U.S. The widespread increases in NH_3 are almost entirely dominated by climate changes across CONUS, with the exception of localized decreases in NH_3 dominated by the transportation emission changes. The increases in T2 across CONUS thermodynamically favors higher NH_3 evasive fluxes and ambient mixing ratios in the future, especially near heavily fertilized crops such as the wheat and corn belts of the U.S. The largest SO_2 changes are mainly dominated by emissions across CONUS, with the exception of parts of the east, southeast, and west U.S. that exhibit climate change dominance. The annual average increases in SO_2 in the east-southeast U.S. are driven by decreases in CFRAC, mainly in the summer, which reduces the amount of in-cloud aqueous chemical reactions that would convert SO_2 to SO_4^{2-}.

CO and NO_x are mainly emissions dominated throughout the seasons, except for CO in the spring and summer, where there are some areas of climate change dominance in CONUS (Figs. S29–S32). VOC changes tend to have their largest areas of climate dominance in the winter and summer seasons, where significant changes in T2 and CFRAC impact the BVOC contributions, while there is more transportation emission dominance in the spring and fall. The largest increases in MDA8 O_3 in the east-northeast U.S. in winter and spring are dominated by emissions and GHGs (i.e., CH_4), but there are regions of climate dominance for the smaller decreases in O_3 across CONUS in summer and fall. NH_3 changes are dominated by climate change during all seasons, especially in the summer, with some areas of enhanced emission contributions in fall to winter season. SO_2 has more emission dominance in the fall and winter, when there are larger emissions of SO_2 from point sources (see max SO_2 emissions in Part I, Figs. S2–S5), which changes to more climate change dominance in the spring and summer, especially where the decreases of CFRAC are the greatest in the summer over CONUS.

Fig. 5 provides similar annual average absolute difference plots of aerosol concentrations as in Fig. 2, but for TT_CC, CC_Only*, and the relative impact ratio of emissions to climate change.

The total $PM_{2.5}$ decreases have contributions from both emissions and climate change, with a slight dominance in emission change impacts. The increases in $PM_{2.5}$ in the west U.S. are dominated by climate changes. The decreases in SO_4^{2-} in the eastern U.S. are strongly dominated by climate changes, and the impacts of reduced CFRAC and in-cloud SO_2 to SO_4^{2-} aqueous chemistry. Although NO_3^- and NH_4^+ have notable impacts from climate including the T2 increases driving less favorable thermodynamic conditions for ammonium nitrate formation, their changes are dominated by emission decreases across CONUS. The decreases in EC are also strongly dominated by emission changes, as EC is generally controlled by direct emissions from combustion sources. The few areas of EC changes due to climate changes in the CC_Only* case are likely due to precipitation and PM wet deposition changes. OM changes, however, are almost entirely controlled by climate changes, where the increases in OM in the west and parts of the southeast U.S. are due to increases in SOA formation dominated by climate-induced BVOC increases stemming from increases in T2 over heavily-vegetated regions. The decreases in OM that are entirely dominated by climate changes are due to higher T2, higher aerosol volatility, and larger partitioning of OM to vapor phase, in spite of the enhanced BVOC emissions.

There is a strong seasonality in the impacts and contribution of climate changes for $PM_{2.5}$ and its species compared to the annual averages (Figs. S33–S37). In regions where climate changes are dominant there are widespread decreases in $PM_{2.5}$ and most species in winter, spring, and fall that are driven by T2 and RT increases, but in summer, the trend reverses and the regions of dominating climate changes show increases in $PM_{2.5}$ and species driven by widespread decrease in RT that reduce wet deposition. For the NO_3^-, NH_4^+, and EC species that show widespread dominance in emission changes, there are more consistently decreasing concentrations across the different seasons.

2.2.3. *Total sulfate and nitrogen deposition*

Considering the importance of future changes in sulfate and nitrogen deposition and their impacts on acidification and eutrophication, Fig. 6 shows the annual average absolute TT_CC and CC_Only* difference plots of dry, wet, and total (dry + wet) deposition for TN and TSO_4^{2-}.

Decreases in total deposition of TSO_4^{2-} in the central and northeastern U.S. is dominated by decreases in wet deposition of SO_4^{2-} from climate change (also see Fig. S38k) driven decreases in both CFRAC and RT (Fig. 3j and l). The increases in wet deposition of TSO_4^{2-} surrounding CONUS are impacted by both increases in CFRAC and RT. The decreases in total deposition of TN in west and east U.S. is driven by decreases in dry deposition of HNO_3 and wet deposition of NO_3^- (comparative analysis not shown). The decreases in dry deposition of TN are clearly dominated by NO_x emission decreases, while the decreases in wet deposition of NO_3^- have strong influences from both emissions and climate. The increases in

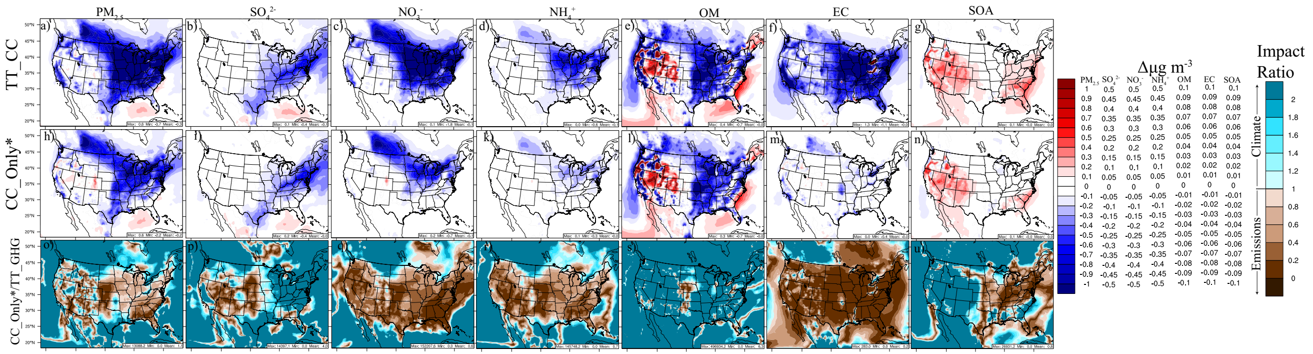

Fig. 5. Spatial absolute (future − current) difference plots of annual (January–December) average concentrations of $PM_{2.5}$, SO_4^{2-}, NO_3^-, NH_4^+, OM, EC, and SOA (row 1; a–g) for TT_CC (row 1; a–f), CC_Only* (row 2; g–l), and an approximate emission vs. climate change impact ratio defined as |ΔCC_Only*|/|ΔTT_GHG| (row 3; m–r) under the A1B scenario. Brown colors indicate dominancy of the impacts of emission changes are dominant, while blue indicates dominancy of the impacts of climate changes. Spatial plots of annual average relative percent changes are shown in Supplementary Fig. S33, and seasonal average relative percent changes are shown in Supplementary Figs. S34–S37. (For interpretation of the references to color in this figure legend, the reader is referred to the Web version of this article.)

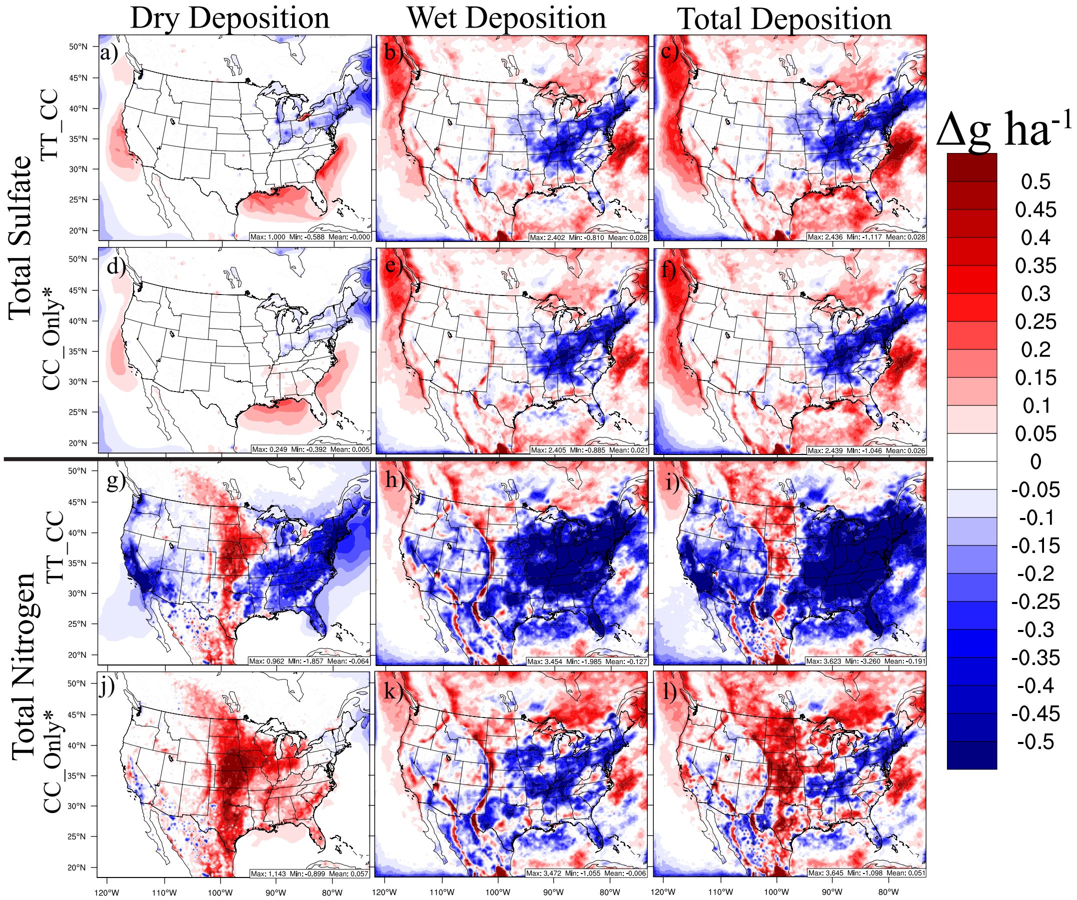
Dry Deposition
Wet Deposition
Total Deposition
Total Sulfate
TT_CC
CC_Only*
Total Nitrogen
TT_CC
CC_Only*
a)
b)
c)
d)
e)
f)
g)
h)
i)
j)
k)
l)
Max: 1.000 Min: -0.588 Mean: -0.000
Max: 2.402 Min: -0.810 Mean: 0.028
Max: 2.436 Min: -1.117 Mean: 0.028
Max: 0.249 Min: -0.392 Mean: 0.005
Max: 2.405 Min: -0.885 Mean: 0.021
Max: 2.439 Min: -1.046 Mean: 0.026
Max: 0.962 Min: -1.857 Mean: -0.064
Max: 3.454 Min: -1.985 Mean: -0.127
Max: 3.623 Min: -3.260 Mean: -0.191
Max: 1.143 Min: -0.899 Mean: 0.057
Max: 3.472 Min: -1.055 Mean: -0.006
Max: 3.645 Min: -1.098 Mean: 0.051
50°N
45°N
40°N
35°N
30°N
25°N
20°N
120°W
110°W
100°W
90°W
80°W
Δg ha^{-1}
0.5
0.45
0.4
0.35
0.3
0.25
0.2
0.15
0.1
0.05
0
-0.05
-0.1
-0.15
-0.2
-0.25
-0.3
-0.35
-0.4
-0.45
-0.5

Fig. 6. Spatial absolute (future − current) 2046–2050 changes in annual (January–December) dry (column 1), wet (column 2), and total deposition (column 3) rates (g ha^{-1}) of TSO_4^{2-} (row 1 and 2) and TN (row 3 and 4) for the TT_CC (row 1, a–c; row 3, g -i) and CC_Only* (row 2, d–f; row 4, j–l) simulations under the A1B scenario. Spatial plots of annual and seasonal average relative percent changes, and the relative climate vs. emission impact ratio are shown in Supplementary Figs. S38 (TSO_4^{2-}) and S39 (TN).

dry deposition of TN from the west north central to the south-southeast U.S. are dominated by climate changes, and are the main contributor to the increases in total deposition of TN in these regions. The strong increases in dry deposition of TN are largely due to relatively strong enhancements in T2 during the summer and fall seasons, higher evaporation of NH_4NO_3 that favors higher partitioning to gas-phase NH_3 concentrations (Fig. 4k), and consequently enhancements in the dry deposition of TN (see footnote 1 for TN definition). We acknowledge there may be other impacts on dry deposition of TN (mainly NH_3) due to changes in V_d in the future climate, which include changes in R_a due to near-surface wind speed changes (see WS10; Fig. 3h), and changes in R_s due to BIDI-NH_3 surface exchange in CMAQ that is a function of soil moisture and canopy/atmospheric temperature changes (see T2; Fig. 3a). As land-use does not change in the future simulations, there are no other impacts to R_s in the calculation of V_d in the future climate scenario presented here. Overall the largest changes in total (but mainly wet) deposition of TSO_4^{2-} are dominated by climate change on an annual and seasonal average basis over CONUS (Fig. S38), with a significant amount of variability in the direction of change that depends on the direction of future seasonal changes in CFRAC and RT (Figs. S24–S27). On an annual average, the regions of the largest decreases in total (both dry and wet) deposition of TN are dominated by emission changes (west and east U.S.), while the largest increases (mainly dry) are dominated by climate changes (Fig. S39k). The NO_x emission decreases dominate TN deposition in winter, but then give way to climate dominance via increased warming, NH_3 concentration, and NH_3 dry deposition enhancements into the summer and fall, especially in the central U.S. (Figs. S39l–S39o).

2.2.4. Emissions vs. greenhouse gas impacts on O_3 and $PM_{2.5}$

The increase in the projected CH_4 background levels in the ORV_GHG, NRE_GHG, TT_GHG, and TT_CC CMAQ simulations lead to increases in the regional O_3 levels, which occurs in conjunction with TT emission impacts on increased local O_3 near urban regions. Production of O_3 occurs as a result of CH_4 oxidation, especially in regions of high NO_x, which includes much of the VOC-limited urban areas of the U.S. where the impacts of TT emission changes on O_3 increases (larger NO_x decreases compared to VOC decreases) are also at their largest. The increase in greenhouse gases in the future also has an impact on CO and VOC levels. Thus in order to better isolate the impacts of TT emissions only, Fig. 7 shows spatial plots of the annual average absolute future changes of CO, VOC, and MDA8 O_3 for the TT_Only (current climate, current GHG, future TT emissions) simulations (Table 1).

The domain-wide mean (minimum) CO decreases (Fig. 7a) are larger at −3.1 ppb (−104.1 ppb) compared to the TT_GHG simulation (Fig. 1s) at −1.0 ppb (−101.5 ppb). There are smaller decreases in VOC for TT_Only (Fig. 7b), however, at a mean (min) of −0.1 ppb (−12.7 ppb) compared to −0.4 ppb (−21.9 ppb) for TT_GHG (Fig. 1u), with the largest decreases in VOC near the VOC-limited (high NO_x) urban regions for TT_GHG. This is because compared to the TT_only simulation, the TT_GHG simulations have higher

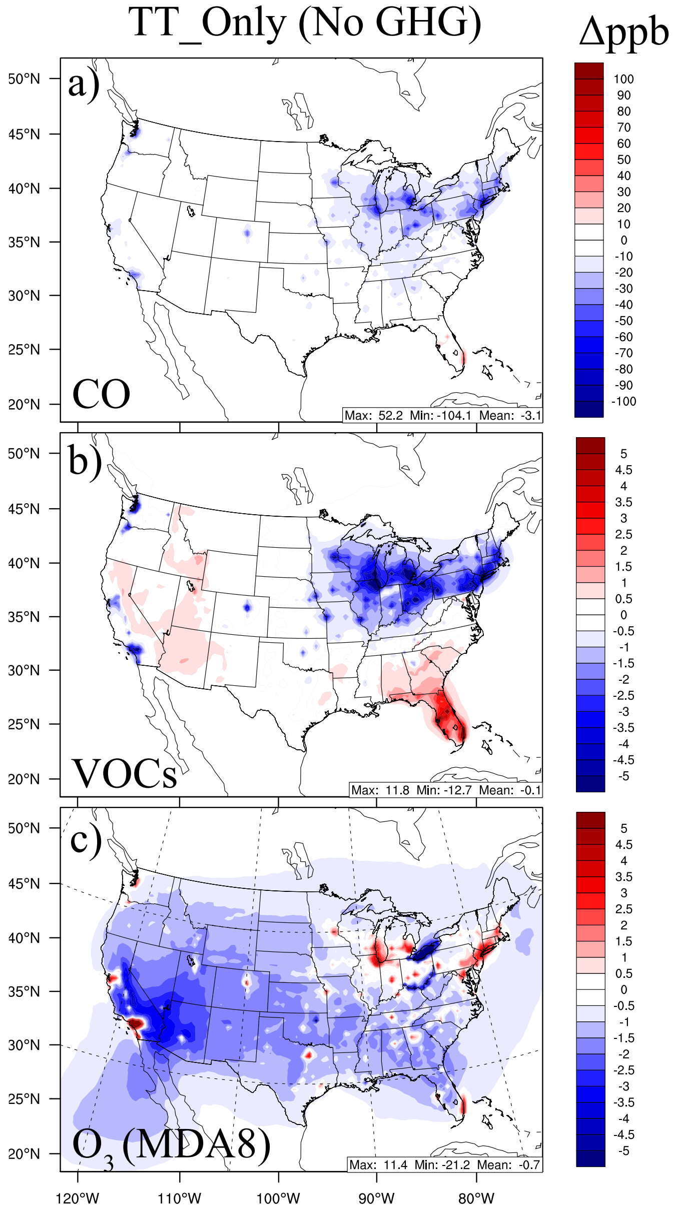

Fig. 7. Spatial absolute (future − current) 2046–2050 changes in annual (January–December) CO (a), VOCs (b), and MDA8 O_3 (c) for TT_Only simulations under the A1B scenario.

levels of CH_4 mixing ratios that enhance the O_3-forming CH_4 chemistry in CMAQ, which includes VOC (i.e., formaldehyde) oxidation and CO production as part of the CH_4 reactions (i.e., the net formaldehyde reaction: $\mathbf{CH_2O} + h\nu + 2O_2 + 2NO \rightarrow \mathbf{CO} + 2OH + 2NO_2 + 2OH + 2NO_2$).

There are stark differences for MDA8 O_3, where TT_Only (Fig. 7c) has a mean decrease of about −0.7 ppb, while TT_GHG (Fig. 1v) has a mean increase of 1.1. Near the VOC-limited urban regions, there are significant increases for both TT_Only and TT_GHG, with localized maximum MDA8 O_3 increases above 10 ppb for some grid cells. It is clear that enhanced background CH_4 in the TT_GHG simulation has a large impact on increasing regional O_3 levels as CH_4 acts directly as a precursor for O_3, and indirectly by enhancing temperature, while the TT_Only simulation highlights the impacts of decreased NO_x emissions on regional (local) O_3 decreases (increases) under static GHGs in the future.

We note that there are negligible differences between the TT_GHG and TT_Only (no GHG) impacts on future on $PM_{2.5}$ and its species concentrations, as it is expected that enhanced CO_2 and CH_4 for the future CMAQ simulations have a minimal direct impact on $PM_{2.5}$. Thus the annual average changes to $PM_{2.5}$ from TT_Only shown in Supplementary Fig. S40 (associated relative and seasonal changes not shown) are nearly identical to those for TT_GHG shown in Fig. 2.

We finally note that the local increases in O_3 shown here are only representative of the projected transportation sector, climate, and background GHG (mainly CH_4) for the IPCC A1B scenario, while all other emission sectors are not projected (i.e., forecasted) to 2046–2050 in this work. Of course, using projected emissions for all other sectors would modify the NO_x-VOC sensitivity for O_3 formation, and thus alter the total regional and local O_3 changes. Likely the local increases in O_3 due to the TT emission changes and NO_x-VOC-O_3 sensitivity, would be dampened by further anthropogenic NO_x and VOC emission decreases from other sectors. Thus while the magnitude of O_3 changes shown here do not represent what the total O_3 changes from all sectors would be, they provide insight as to how the transportation sector emission changes may play a role (through NO_x-VOC-O_3 sensitivity) in potential O_3 increases in the future. In fact, future increases in O_3 over the U.S. has been demonstrated in previous work that includes climate, GHG, and emission changes and their interactions with O_3 changes under different scenarios (e.g., Tao et al., 2007; Racherla and Adams, 2009; He et al., 2016).

2.2.5. *Implications of future O_3 and $PM_{2.5}$ levels over the U.S.*

Fig. 8 shows cumulative distribution functions (CDF) of MDA8 O_3 mixing ratios and daily 24-hr average (DA24) $PM_{2.5}$ concentrations for the CURR, TT_Only (emission changes only), TT_GHG (emission + GHG changes), and TT_CC (emission + climate + GHG changes) simulations across the nine climate regions in the U.S. as defined by the National Climatic Data Center (NCDC)[6] (i.e., Northeast, Southeast, Upper Midwest, Central, South, West North Central, Southwest, Northwest, and West).

There is a wide range in variability in the impacts of emissions, GHG, and climate on the CDFs from the current to future scenarios across the nine CONUS regions. In the Northwest (Fig. 8e), West (Fig. 8g), and Northeast (Fig. 8q) there are slight increases (decreases) at relatively low (high) O_3 mixing ratios for TT_Only and TT_GHG, but there are notable decreases at all O_3 mixing ratios for TT_CC (CDF shifted to the left of CURR). This demonstrates the dominance of climate change on the future decreases of MDA8 O_3, and an increase in its impact at the higher end of O_3 mixing ratios (i.e., the CDF for TT_CC steepens as mixing ratios increase to ~ 60 ppb). In other regions such as the Southwest (Fig. 8i), West North Central (Fig. 8a), Upper Midwest (Fig. 8c), and Central (Fig. 8o), however, there are increases in the MDA8 O_3 CDFs for TT_Only, TT_GHG, and TT_CC relative to CURR, while the TT_CC increases are comparatively less due to the effects of climate change on O_3 discussed earlier. In fact, the CDFs for TT_CC shift closer to the CURR at higher MDA8 O_3 mixing ratios (>40 ppb), especially in the Upper Midwest. The CDFs decrease for all simulations in the Southeast, with progressively less decrease from TT_Only, TT_GHG, and TT_CC. In the South, there is minimal change in TT_Only and TT_GHG at the lower O_3 mixing ratios, while exhibiting slight decreases at the higher, while TT_CC is consistently the largest decreases across all O_3 mixing ratios. The trend in larger decreases in MDA8 O_3 at higher O_3 mixing ratios is similar between the South and Southeast.

---

[6] https://www.ncdc.noaa.gov/monitoring-references/maps/us-climate-regions.php.

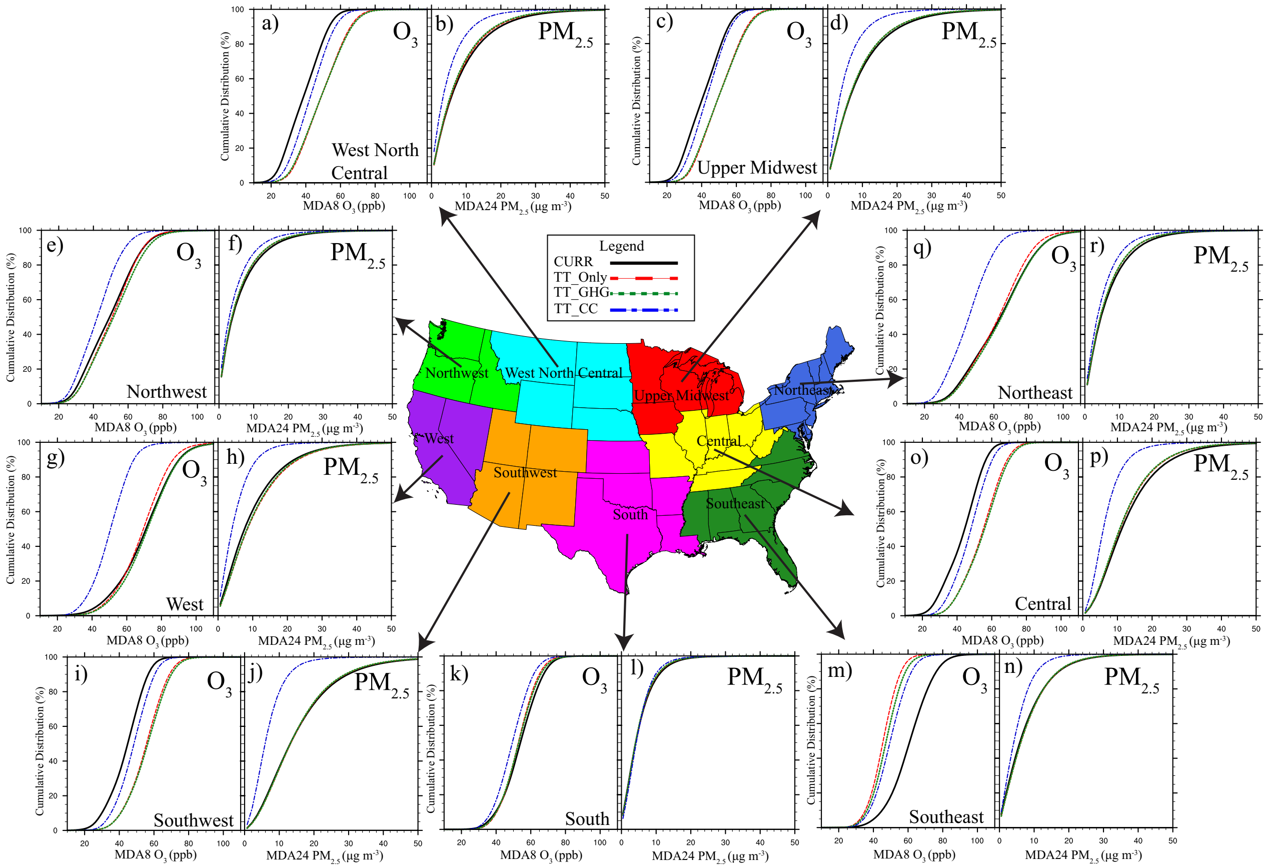

Fig. 8. Cumulative distribution function (CDF) curves (%) of MDA8 O_3 and DA24 $PM_{2.5}$ for the CURR (black), TT_Only (red), TT_GHG (green), and TT_CC (blue) simulations across the nine NCDC climate regions in the U.S. including West North Central (a–b), Upper Midwest (c–d), Northwest (e–f), West (g–h), Southwest (i–j), South (k–l), Southeast (m–n), Central (o–p), and Northeast (q–r) regions. (For interpretation of the references to color in this figure legend, the reader is referred to the Web version of this article.)

There is significantly less variability in the $PM_{2.5}$ CDFs for TT_Only, TT_GHG, and TT_CC changes across the nine regions of CONUS in Fig. 8. There are minimal changes for TT_Only and TT_GHG compared to CURR in each of the regions, which is consistent with the small domain-wide average relative percent decrease in $PM_{2.5}$ in CONUS (~−5.0%; Fig. S6v). There are consistently larger decreases in the $PM_{2.5}$ CDFs from climate impacts in TT_CC, with the smallest to largest decreases found in the following order: South (Fig. 8l), Northwest (Fig. 8f), Northeast (Fig. 8r), West North Central (Fig. 8b), Southeast (Fig. 8n), Upper Midwest (Fig. 8d), West (Fig. 8h), Central (Fig. 8p), and Southwest (Fig. 8j). The large disparity in $PM_{2.5}$ CDFs for TT_CC is caused by a combination of effects from changes in both T2 and RT across each defined region in CONUS. Widespread T2 increases impact the decreased $PM_{2.5}$ CDF for TT_CC, but some regions experience decreases in RT (i.e., precipitation) that mitigates wet deposition rates and the resulting $PM_{2.5}$ decreases (e.g., South), while others experience increased RT that leads to enhanced $PM_{2.5}$ decreases (e.g., West and Southwest).

3. Summary and discussion

The application of dynamic technology emission projections (Part I; Campbell et al., 2018) and downscaled climate/air quality modeling, i.e., the Technology-Driver Model presented here, has led to new and important impacts on (and policy implications of) detailed transportation emission control to help attain, maintain, or improve future air quality. For the projected air quality changes over the U.S. due to transportation emission changes by 2046–2050, there are widespread decreases in CO (avg. ~ −1 ppb or −1%) and NO_x (avg. − 0.3 ppb or −26%) due to dominating decreases in on-road vehicle emissions; however, there are increases in O_3 (avg. ~ +1 ppb or +2.4%) across eastern U.S. due to 1) enhanced CH_4 concentrations (not shown) and 2) larger NO_x emission reduction than VOC emission reduction over VOC-limited regions. The lower O_3 in the western U.S. is impacted by widespread decreases in NO_x emissions. There are also decreases in SO_2 and NH_3 due to decreasing on-road vehicle emissions near the urban centers, as well as decreases in NO_x and SO_2 in the western U.S. from decreased locomotive emissions near major railways. Thus there are clear indications of a strong impact of projected dynamic technology transportation emissions on future U.S. air quality, such as reductions in CO, VOCs, and NO_x, but enhancements in O_3 mixing ratios, which has large spatial and seasonal variability.

There are widespread but comparatively smaller decreases in $PM_{2.5}$ concentrations (avg. ~ −0.2 μg m^{-3} or −5.0%), with a max of −2.4 μg m^{-3}, which is largely due to decreased NH_4^+ and NO_3^- formation from on-road vehicle NO_x and NH_3 emission reductions, as well as on-road vehicle and non-road engine decreases in primary elemental carbon emissions. Supplementary analyses show that the decrease in total $PM_{2.5}$ due to emission decreases also leads to an associated reduction in haze, especially in the upper Midwest, Central, and Northeast U.S., with an improvement in visibility (ave. ~ -0.2 dv) as large as -2 dv. The decreases in EC, as well as some increases in total organic matter in the eastern U.S., lead to predominantly increasing primary organic to elemental carbon ratio, $(OC/EC)_{pri}$.

Further supplementary analyses indicate that on-road vehicle and non-road engine emission and greenhouse gas changes lead to widespread decreases and increases in dry deposition of SO_2 and O_3, respectively, both which follow closely the changes in their projected gas concentrations for the ORV_GHG, NRE_GHG, and TT_GHG simulation cases. The decreases in NO_x emissions from on-road vehicles and non-road engines lead to decreases in both dry and wet deposition of total nitrogen, which are largely due to decreases in dry deposition of HNO_3 and wet deposition of NO_3^-. Decreases in on-road vehicle NH_3 emissions also lead to decreases in the dry deposition of NH_3 and wet deposition of NH_x.

Generally, the future 2046–2050 A1B climate over the U.S. is typical of 1) warmer temperatures, with exceptions of some regions of the southern U.S. in the winter, 2) faster near-surface wind speeds and a more unstable/deeper boundary layer heights in all seasons (most prolific in winter), and 3) wetter and cloudier conditions in the west and northwest during the winter and spring, and in most of the U.S. in the fall, but drier and less cloudy conditions in the southeast, with widespread decreases in clouds and precipitation in the summer. The climate changes lead to 1) increases in 2-m temperature and downward shortwave radiation that may enhance biogenic VOCs and lead to increased O_3 and $PM_{2.5}$ levels over some regions, especially in the western U.S., 2) increases in the boundary layer height that can lead to decreases in O_3 (and other species) to first order, especially in the eastern U.S., and 3) increases (decreases) in total rain and wet deposition that decrease (increase) $PM_{2.5}$ concentrations in the west and northwest (south and southeast) U.S.

Transportation emission changes dominate the CO and NO_x concentration decreases, climate changes dominate the total VOC changes, emissions and greenhouse gas (i.e., CH_4) changes dominate increases in O_3, while climate changes mitigate (enhance) these O_3 increases in eastern (northwest) U.S., and both emission and climate changes contribute approximately equally to the widespread total $PM_{2.5}$ decreases, especially in the east and west U.S. The decreases in SO_4^{2-}, both increases and decreases in organic matter, and the increases in secondary organic aerosol are dominated by climate changes, while the decreases in NO_3^-, NH_4^+, and elemental carbon are dominated by transportation emission changes. The decreases in total deposition of total SO_4^{2-} in the central and northeastern U.S. are driven by decreases in wet deposition of SO_4^{2-} from mainly climate changes. The decreases in the total deposition of nitrogen in west and east U.S. are driven by decreases in dry (wet) deposition of HNO_3 (NO_3^-) from mainly NO_x emission decreases. The increases in total deposition of nitrogen from the west north central to south U.S. are due to increases in dry deposition of NH_3 driven by climate changes (significant temperature increases in summer and fall).

Importantly, changing the transportation emissions only (current greenhouse gas levels) leads to widespread decreases in regional O_3, except for increases in O_3 near VOC-limited regions with a maximum increase for a specific grid cell of about +11 ppb. Increasing the projected CH_4 concentration enhances CH_4 chemistry in CMAQ, which in turn leads to large increases in the regional O_3, and relatively smaller increases in CO and decreases in VOCs. There are negligible direct impacts of increasing background CO_2 or CH_4 on $PM_{2.5}$ or its species concentrations.

The cumulative distribution functions for the maximum daily average 8-hr O_3 show significant variability in the relative changes in TT_Only, TT_GHG, and TT_CC simulations depending on the specific U.S. region (and U.S. state), while the daily 24-hr average $PM_{2.5}$ distributions show very small and consistent changes in TT_Only and TT_GHG, but larger decreases for TT_CC that have some variability in the different regions. Over the nine U.S. regions, there is a decrease in the future O_3 levels when considering TT_Only changes, consistent O_3 increases from TT_GHG changes, and either minimal change or increases of O_3 for TT_CC.

When considering hypothetical impacts of future transportation sector emissions only, there is a decrease in percentage of maximum daily average 8-hr O_3 values exceeding O_3 standards in all nine CONUS regions for TT_Only, except near local VOC-limited areas where O_3 increases (Supplementary Section 6; Tables S1 and S2). Increasing the CH_4 level in TT_GHG increases the percentage of O_3 above the hypothetical thresholds, and incorporating climate change reduces the percentage while compensating the increases from emissions and CH_4 changes. There are consistent decreases in the percentage of daily 24-hr average $PM_{2.5}$ values exceeding hypothetical future $PM_{2.5}$ standards, which are impacted both by transportation emissions (TT_Only and TT_GHG) and future climate change (TT_CC) (Supplementary Section 6; Tables S3 and S4). Results from this work would be very useful in supporting the policy and regulatory analysis and assessment of the impacts of future control and changes in transportation emissions on U.S. air quality in the face of imminent climate changes.

Acknowledgements

This study is funded by the National Science Foundation Earth System Model (EaSM) program (AGS-1049200) at North Carolina State University, and the United States Department of Agriculture EaSM program (2012-67003-30192) at the University of Chicago/Argonne National Laboratory. This research used resources of the National Energy Research Scientific Computing Center (NERSC), a Department of Energy (DOE) Office of Science User Facility supported by the Office of Science of the U.S. DOE under Contract No. DE-AC02-05CH11231. Specifically, the NERSC Hopper (retired), Edison, and Cori computing systems were used to perform the WRF and WRF-CMAQ simulations. The meteorological initial and boundary conditions for the current-year and future-year WRF periods were provided by NCAR's Community Climate System Model (CCSM). The initial and boundary conditions from CCSM were further processed by Ruby Leung's group at the Pacific Northwest National Laboratory for dynamical downscaling.

Appendix A. Supplementary data

Supplementary data related to this article can be found at https://doi.org/10.1016/j.envpol.2018.03.016.

References

Arora, S., Vyas, A., Johnson, L.R., 2011. Projections of highway vehicle population, energy demand, and CO2 emissions in India to 2040. Nat. Resour. Forum 35, 49–62.

Baklanov, A., Collins, B., Folberth, G., Gauss, M., Gonzalez-Aparicio, I., Jonson, J.E., Haugen, J.E., Kong, X., Mahura, A., Nuterman, R., Nyiri, A., Simpson, D., Soares, J., Sofiev, M., Sokhi, R., Theloke, J., Tsyro, S., Zakey, A., 2010. Interaction between Pollution and Climate for Future Transport Scenarios, Seventh Framework Programme, ENV.2009.1.2.2.1 Transport Related Air Pollution and Health Impacts.

Bash, J.O., Cooter, E.J., Dennis, R.W., Walker, J.T., Pleim, J.E., 2013. Evaluation of a regional air-quality model with bi-directional NH3 exchange coupled to an agro-ecosystem model. Biogeosciences 10, 1635–1645. https://doi.org/10.5194/bg-10-1635-2013.

Bickford, E., 2012. Emissions and Air Quality Impacts of Freight Transportation. Ph.D. Dissertation. University of Wisconsin-Madison, 154 pp.

Cabada, J.C., Pandis, S.N., Subramanian, R., Robinson, A.L., Polidori, A., Turpin, B., 2004. Estimating the secondary organic aerosol contribution to $PM_{2.5}$ using the EC tracer method. Aerosol Sci. Technol. 38, 140–155. https://doi.org/10.1080/02786820390229084.

Campbell, P., Zhang, Y., Yahya, K., Wang, K., Hogrefe, C., Pouliot, G., Knote, C., Hodzic, A., San Jose, R., Perez, J., Guerrero, P.J., Baro, R., Makar, P., 2015. A multi-model assessment for the 2006 and 2010 simulations under the air quality model evaluation international initiative (AQMEII) phase 2 over North America: Part I. Indicators of the sensitivity of O3 and PM2.5 formation regimes. Atmos. Environ. 115, 569–586. https://doi.org/10.1016/j.atmosenv.2014.12.026.

Campbell, P., Zhang, Y., Yan, F., Lu, Z., Streets, D., 2018. Impacts of transportation sector emissions on future U.S. air quality in a changing climate. Part I: projected emissions, simulation design, and model evaluation. Environ. Pollut. (submitted for publication).

Colvile, R., Hutchinson, E., Mindell, J., Warren, R., 2001. The transport sector as a source of air pollution. Atmos. Environ. 35 (9), 1537–1565.

Cooter, E.J., Bash, J.O., Benson, V., Ran, L.-M., 2012. Linking agricultural management and air-quality models for regional to national-scale nitrogen deposition assessments. Biogeosciences 9, 4023–4035. https://doi.org/10.5194/bgd-9-6095-2012.

EPA, 2007. Guidance on the Use of Models and Other Analyses for Demonstrating Attainment of Air Quality Goals for Ozone, PM2.5, and Regional Haze, 454/B-07–002. Research Triangle Park, North Carolina.

European Environmental Agency (EEA), 2012. Greenhouse Gas Emission Trends and Projections in Europe 2012. EEA Report No 6/2012, 164 pp.

Eyring, V., Isaksen, I.S.A., Berntsen, T., Collins, W.J., Corbett, J.J., Endresen, O., Grainger, R.G., Moldanova, J., Schlager, H., Stevenson, D.S., 2010. Transport impacts on atmosphere and climate: shipping. Atmos. Environ. https://doi.org/10.1016/j.atmosenv.2009.04.059. https://www.sciencedirect.com/science/article/pii/S1352231009003379.

Ghosh, R., Lurmann, F., Perez, L., Penfold, B., Brandt, S., Wilson, J., Milet, M., Künzli, N., McConnell, R., 2016. Near-roadway air pollution and coronary heart disease: burden of disease and potential impact of a greenhouse gas reduction strategy in Southern California. Environ. Health Perspect. 124, 193–200. https://doi.org/10.1289/ehp.1408865.

He, H., Liang, X.-Z., Le, H., Wuebbles, D.J., 2016. Future U.S. ozone projections dependence on regional emissions, climate change, long-range transport and differences in modeling design. Atmos. Environ. 128, 124–133.

International Energy Agency (IEA), 2014. Harnessing electricity's potential. Energy Technol. Perspect. 2014, 382 pp.

Lee, D.S., Pitari, G., Grewe, V., Gierens, K., Penner, J.E., Petzold, A., Prather, M., Schumann, U., Bais, A., Iachetti, D., Berntsen, T., Lim, L.L., Sausen, R., 2010. Transport impacts on atmosphere and climate: aviation. Atmos. Environ. 40, 4678–4734.

Li, H., Li, L., Huang, C., An, J., Yan, R., Huang, H., Wang, Y., Lu, Q., Wang, Q., Lou, S., et al., 2015. Ozone source apportionment at urban area during a typical photochemical pollution episode in the summer of 2013 in the Yangtze River Delta. Environ. Sci. 36, 1–10.

McDonald-Buller, E.C., Webb, A., Kockelman, K.M., Zhou, B., 2010. Effects of transportation and land use policies on air quality. J. Transp. Res. Board 2158, 28–35.

Moss, R.H., Edmonds, J.A., Hibbard, K., Manning, M., Rose, S.K., van Vuuren, D.P., Carter, T.R., Emori, S., Kainuma, M., Kram, T., Meehl, G., Mitchell, J., Nakicenovic, N., Riahi, K., Smith, S., Stouffer, R.J., Thomson, A., Weyant, J., Wilbanks, T., 2010. The next generation of scenarios for climate change research and assessment. Nature 463, 747–756.

Nakicenovic, N., Alcamo, J., Davis, G., de Vries, B., Fenhann, J., Gaffin, S., Gregory, K., Grübler, A., Jung, T.Y., Kram, T., La Rovere, E.L., Michaelis, L., Mori, S., Morita, T., Pepper, W., Pitcher, H., Price, L., Riahi, K., Roehrl, A., Rogner, H., Sankovski, A., Schlesinger, M., Shukla, P., Smith, S., Swart, R., van Rooijen, S., Victor, N., Zhou, D., 2000. Special Report on Emissions Scenarios: a Special Report of Working Group III of the Intergovernmental Panel on Climate Change. Cambridge University Press, Cambridge, New York.

Penrod, A., Zhang, Y., Wang, K., Wu, S.-Y., Leung, L.R., 2014. Impacts of future climate and emission changes on U.S. air quality. Atmos. Environ. 89, 533–547. https://doi.org/10.1016/j.atmosenv.2014.01.001.

Pitchford, M.L., Malm, W.C., 1994. Development and application of a standard visual index. Atmos. Environ. 28, 1049–1054.

Pleim, J.E., Ran, L., 2011. Surface flux modeling for air quality applications. Atmosphere 2, 271–302. https://doi.org/10.3390/atmos2030271.

Pleim, J.E., Xiu, A., Finkelstein, P.L., Otte, T.L., 2001. A coupled land-surface and dry deposition model and comparison to field measurements of surface heat, moisture, and ozone fluxes. Water Air Soil Poll. Focus 1, 243–252.

Racherla, P.N., Adams, P.J., 2009. U.S. ozone air quality under changing climate and anthropogenic emissions. Environ. Sci. Technol. 43, 571–577. https://doi.org/10.1021/es800854f.

Rogelj, J., Meinshausen, M., Knutti, R., 2012. Global warming under old and new scenarios using IPCC climate sensitivity range estimates. Nat. Clim. Change 2, 248–253. https://doi.org/10.1038/nclimate1385.

Saikawa, E., Kurokawa, J., Takigawa, M., Borken-Kleefeld, J., Mauzerall, D.L., Horowitz, L.W., Ohara, T., 2011. The impact of China's vehicle emissions on regional air quality in 2000 and 2020: a scenario analysis. Atmos. Chem. Phys. 11, 9465–9484. https://doi.org/10.5194/acp-11-9465-2011.

Tao, Z., Williams, A., Huang, H.-C., Caughey, M., Liang, X.-Z., 2007. Sensitivity of U.S. surface ozone to future emissions and climate changes. Geophys. Res. Lett. 34, L08811. https://doi.org/10.1029/2007GL029455.

Turpin, B.J., Huntzicker, J.J., 1995. Identification of secondary organic aerosol episodes and quantification of primary and secondary organic aerosol concentrations during SCAQS. Atmos. Environ. 29 (3), 3527–3544. https://doi.org/10.1016/1352-2310(94)00276-Q.

Turpin, B.J., Huntzicker, J., Larson, S.M., Cass, G.R., 1991. Los Angeles summer midday particulate carbon: primary and secondary aerosol. Environ. Sci. Technol. 25, 1788–1793. https://doi.org/10.1021/es00022a017.

Uherek, E., Halenka, T., Borken-Kleefeld, J., Balkanski, Y., Berntsen, T., Borrego, C., Gauss, M., Hoor, P., Juda-Rezler, K., Lelieveld, J., 2010. Transport impacts on atmosphere and climate: land transport. Atmos. Environ. 44, 4772–4816.

Viana, M., Hammingh, P., Colette, A., Querol, X., Degraeuwe, B., Vlieger, I., de vanAardenne, J., 2014. Impact of maritime transport emissions on coastal air quality in Europe. Atmos. Environ. 90, 96e105. https://doi.org/10.1016/j.atmosenv.2014.03.046.

Vijayaraghavan, K., Lindhjem, C., DenBleyker, A., Nopmongcol, U., Grant, J., Tai, E., Yarwood, G., 2012. Effects of light duty gasoline vehicle emission standards in the United States on O3 and particulate matter. Atmos. Environ. 60, 109–120. https://doi.org/10.1016/j.atmosenv.2012.05.049.

Wu, C., Yu, J.Z., 2016. Determination of primary combustion source organic carbon-to-elemental carbon (OC/EC) ratio using ambient OC and EC measurements: secondary OC-EC correlation minimization method. Atmos. Chem. Phys. 16, 5453–5465. https://doi.org/10.5194/acp-16-5453-2016.

Yahya, K., Campbell, P., Zhang, Y., 2017. Decadal application of WRF/chem for regional air quality and climate modeling over the U.S. under the representative concentration pathways scenarios. Part 2: current vs. future simulations. Atmos. Environ. 152, 584–604. https://doi.org/10.1016/j.atmosenv.2016.12.028. https://www.sciencedirect.com/science/article/pii/S1352231016310044.

Yan, F., Winijkul, E., Streets, D.G., Lu, Z., Bond, T.C., Zhang, Y., 2014. Global emission projections for the transportation sector using dynamic technology modeling. Atmos. Chem. Phys. 14 https://doi.org/10.5194/acp-14-5709-2014, 5790–5733.